photonics

MDPI

Article

Photodetector Based on Twisted Bilayer Graphene/Silicon Hybrid Slot Waveguide with High Responsivity and Large Bandwidth

Siqi Yan [1,*], Ze Zhang [1], Weiqin Wang [1], Ziwen Zhou [1], Wenyi Peng [1], Yifan Zeng [1], Yuqin Yuan [1], Siting Huang [1], Xuchen Peng [1], Xiaolong Zhu [2], Ming Tang [1] and Yunhong Ding [3,*]

[1] School of Optical and Electronic Information, Huazhong University of Science and Technology, Wuhan 430074, China
[2] State Key Laboratory of Precision Spectroscopy, School of Physics and Electronic Science, East China Normal University, Shanghai 200241, China
[3] DTU Fotonik, Department of Photonics Engineering, Technical University of Denmark, DK-2800 Kongens Lyngby, Denmark
* Correspondence: siqya@hust.edu.cn (S.Y.); yudin@fotonik.dtu.dk (Y.D.)

Abstract: Graphene/silicon hybrid photodetector operating at communication wavelength has attracted enormous attention recently due to its potential to realize bandwidth larger than 100 GHz. However, the responsivity is intrinsically limited by the low absorption from the atomic-thick graphene monolayer, which imposes significant obstacles towards its practical application. Although plasmonic structures has been widely applied to enhance the responsivity, it may induce the metallic absorption thus limit the responsivity lower than 0.6 A/W. Twisted bilayer graphene (TBG) has been reported to hold the ability to dramatically enhance the optical absorption due to the unique twist-angle-dependent van Hove singularities. In this article, we present a design of a silicon/TBG hybrid photodetector with a responsivity higher than 1 A/W and bandwidth exceeding 100 GHz. The enhanced responsivity is achieved by tuning the twisted angle of TBG to increase the absorption within the 1550 nm as well as utilizing the silicon slot waveguide to boost the mode overlap with TBG. The fabrication process of proposed design is also discussed demonstrating the advantages of low fabrication complexity. The proposed silicon/TBG photodetector could not only exhibit superior performance compared to previously reported silicon/monolayer graphene photodetector, but also pave the way for the practical application of graphene-based silicon optoelectronic devices.

Keywords: silicon photodetector; twisted bilayer graphene; silicon photonics

check for updates

Citation: Yan, S.; Zhang, Z.; Wang, W.; Zhou, Z.; Peng, W.; Zeng, Y.; Yuan, Y.; Huang, S.; Peng, X.; Zhu, X.; et al. Photodetector Based on Twisted Bilayer Graphene/Silicon Hybrid Slot Waveguide with High Responsivity and Large Bandwidth. *Photonics* **2022**, *9*, 867. https://doi.org/10.3390/photonics9110867

Received: 23 October 2022
Accepted: 15 November 2022
Published: 17 November 2022

Publisher's Note: MDPI stays neutral with regard to jurisdictional claims in published maps and institutional affiliations.

Copyright: © 2022 by the authors. Licensee MDPI, Basel, Switzerland. This article is an open access article distributed under the terms and conditions of the Creative Commons Attribution (CC BY) license (https://creativecommons.org/licenses/by/4.0/).

1. Introduction

Owing to the unprecedented development of the data-driven novel technology such as Cloud Computing, Internet of Things, and Big Data Analytics, the optical communication systems are expected to feature ultrahigh bandwidth in order to support the transmission of the explosive amount of data [1,2]. As a key building block of the optical communication systems, the integrated photodetectors are required to exhibit extraordinary performances including ultra-large bandwidth above 100 GHz as well as the high responsivity larger than 1 A/W, which remains challenging to be achieved simultaneously within the conventional-material-based platforms at the communication wavelength [3]. Until recently, a Ge/Si photodetector with bandwidth up to 265 GHz was demonstrated, but its external responsivity is only 0.2 A/W [4]. The fastest InP-based photodetector has a bandwidth of 170 GHz while the responsivity is limited to 0.27 A/W [5]. Because of the unique band linearly dispersive and gapless band structure, graphene has been considered as an ideal material to be integrated with silicon photonics circuit, in order to realize ultrafast on-chip photodetection [5–10]. The hybrid silicon/graphene photodetectors have been widely reported to possess a bandwidth higher than 100 GHz. However, most of these photodetectors suffer from low responsivity due to the weak absorption within the monolayer graphene.

Although various photonic structures including photonic crystal structures, plasmonic structures have been proposed to boost the responsivity, the highest value of the responsivity working within the 1550 nm wavelength range is still lower than 0.7 A/W, which could hardly compete with the commercial photodetectors [8,11–13]. Therefore, the main motivation of our work is to design a photodetector that holds bandwidth higher than 100 GHz and responsivity larger than 1 A/W simultaneously.

Twisted bilayer graphene (TBG) is non-AB stacked bilayer graphene and has recently attracted numerous interests because of its impressive optical and electronic properties [14–16]. Specially, the TBG has exhibited a significant enhanced optical absorption well exceeding the linear-band absorption of two layers of monolayer graphene, due to the presence of van Hove singularities (vHSs) [17]. This novel property results in graphene photodetectors with enhanced responsivity operating at visible and mid-infrared wavelength range [18–20]. In this work, we design a silicon/TBG photodetector operating at the communication wavelength range, featuring both high responsivity and large bandwidth simultaneously. We first calculate the specific twist angle that enhances the absorption within 1550 nm. Afterwards, we optimize the silicon/TBG hybrid waveguide structures to ensure large mode overlap as well as large bandwidth. Finally, we provide a thorough discussion about the fabrication process of the potential silicon/TBG photodetector. We expect the proposed silicon/TBG hybrid photodetector can outperform the reported silicon/graphene photodetectors and pave the way for practical applications of TBG in the optical communication area.

2. Device Design and Theoretical Calculation

2.1. The Theoretical Model of the TBG

To realize the responsivity enhancement within the TBG at the wavelength of 1550 nm, the photon energy of the incident light is expected to be equaled to the energy interval of the two vases of TBG, as the Equation (1) displays:

$$\Delta E_{VHS} = \frac{hc}{\lambda} \tag{1}$$

where h is the Planck constant, c is the speed of light in the vacuum, λ is the wavelength of the incident light, and thus ΔE_{VHS} is the energy interval of the vases within the band structure of the TBG. Noted that when the rotation angle is small, the mismatch between the lattice vectors of the two layers gives rise to a Moire' pattern. The value of the ΔE_{VHS} is strongly affected by the twisted Moire' angle θ and can be described by Equation (2) for simplicity [21]:

$$\Delta E_{VHS} = 2V_F\hbar\frac{4\pi}{3a}\sin(\theta/2) - 2t_\theta \tag{2}$$

in which $V_F = 10^6$ m/s is the proposed Fermi velocity, $\hbar$ is the reduced Planck constant, $a = 0.246$ nm is the lattice constant of the monolayer graphene, and $t_\theta = 0.1$ eV is the interlayer transition parameter reflecting the coupling strength between the monolayer [21]. The relationship between the θ and the ΔE_{VHS} is shown in Figure 1. We can find that when λ is set as 1550 nm, θ is calculated to be 5.2°.

2.2. The Design of Silicon/TBG Hybrid Photodetector

The schematic of the silicon/TBG photodetector is shown in Figure 2. The photodetector includes a silicon slot waveguide, two layers of monolayer graphene with a specific twisted angle θ covering the slot region, as well as two electrodes collecting the carriers within the graphene. The photodetector is realized on a commercial Silicon-on-Insulator (SOI) platform with the top silicon layer of thickness t_{Si} and the buried oxide layer of thickness t_{ox}. Normally, there are three types of combination (t_{Si}, t_{ox}) of t_{Si} and t_{ox} available for the SOI wafer, which are (260 nm, 1 μm), (250 nm, 3 μm), (220 nm, 2 μm) and can be designated as type-A, type-B, type-C respectively. The performance of silicon/TBG photodetector based on these three different types of wafers will be discussed later. In

our design, the light is confined within the silicon slot waveguide with the slot width of g and slab width of ω while the TBG is on top of the slot waveguide. The silicon slot waveguide is employed to guide light into the absorption region since it could enhance the light-TBG interaction and thus boosting the performance of the photodetector, as the inset shows. The filling material of the slot waveguide is SiO_2. A 10 nm aluminum oxide layer is inserted between the slot waveguide and the TBG, which is not shown in Figure 2 in order to highlight the TBG. Moreover, two electrodes (100 nm Au/ 5 nm Ti) are deposited on the top of the TBG with the distance of d.

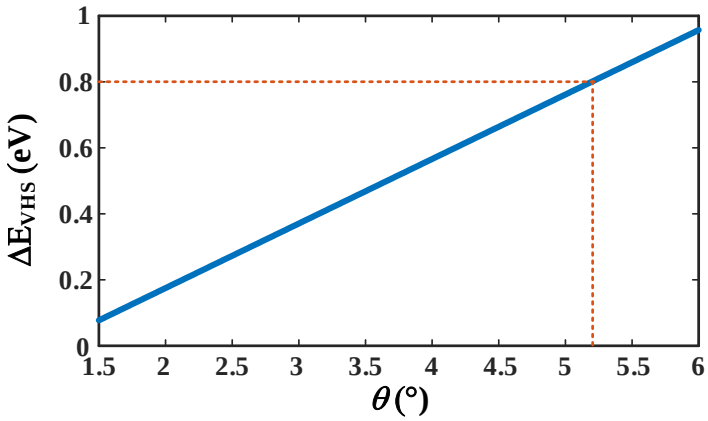

Figure 1. The relationship between the energy interval of VHSs and the twisted angle.

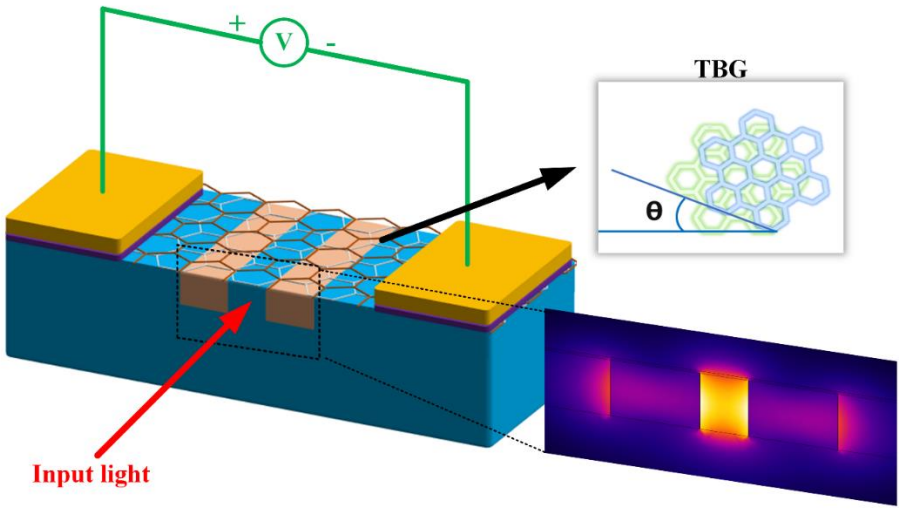

Figure 2. The schematic and the mode distribution of the TBG/silicon hybrid photodetector.

2.3. The Responsivity Calculation of the Silicon/TBG Photodetector

To obtain the responsivity of the silicon/TBG structure, the light absorption within the TBG is first calculated by the following process: The TBG is modelled as a surface current and its surface conductivity σ_{TBG} can be described by the equations below [17]:

$$\sigma_{TBG} = 2\sigma_{mono} + \sigma_{\alpha} \quad (3)$$

In which σ_{mono} is the conductivity of the monolayer graphene and σ_{α} is the angle-dependent conductivity enhancement originated from the twisted bilayer graphene, which is due to the enhanced density of states (DOS) close to the top of the moiré Dirac bands and the bottom of the empty bands. The σ_{mono} can be calculated by the following equation [11]:

$$\sigma_{mono} = \frac{-je^2}{\pi\hbar^2(\omega + j2\Gamma)}\int_0^\infty \zeta\left(\frac{\partial f_d(\zeta)}{\partial\zeta} - \frac{\partial f_d(-\zeta)}{\partial\zeta}\right)d\zeta + \frac{j(\omega + j2\Gamma)}{\pi\hbar^2}\int_0^\infty \zeta\left(\frac{f_d(-\zeta) - f_d(\zeta)}{(\omega + j2\Gamma)^2 - 4\left(\frac{\zeta}{\hbar}\right)^2}\right)d\zeta \quad (4)$$

In Equation (4), the first term represents intraband contributions while the second term represents interband contributions. $f_d(\zeta) = \left[e^{(\zeta-\mu_c)/K_BT} + 1\right]^{-1}$ is the Fermi-Dirac distribution, and ω is the angular frequency of the photon. Γ represents the scattering rate. μ_c is the chemical potential of graphene. T is the temperature. e is the electron charge and k_B is the Boltzmann constant.

The conductivity enhancement σ_α can be calculated as the Equation (5) shows [17]:

$$\sigma_\alpha(\omega) = \frac{S_\alpha}{\sqrt{2\pi\Gamma_\alpha^2}}\exp\left[-\frac{(\hbar\omega - E_\alpha)^2}{2\Gamma_\alpha^2}\right] \quad (5)$$

where S_α, E_α and Γ_α represents the intensity, energy, and broadening of the conductivity enhancement respectively. It should be noted that in this work, we mainly focus on the light absorption property of the TBG with relatively large twist so the modeling of the TBG is simplified. In fact, plenty of factors including twist angle, doping level as well as the temperature can significantly impacts the band structure of the TBG [19,22,23]. One should fully consider all these factors when establishing a more accurate model of TBG.

We use the Finite Element Method (FEM) to calculate the transvers-electric (TE) mode distribution of the silicon/TBG hybrid waveguide and the TBG absorption coefficient α_{TBG}. In the calculation, the refractive indices of the materials are set as below: n_{Si} = 3.47, n_{SiO2} = 1.45, n_{Al2O3} = 1.66, n_{Ti} = 3.43 + 3.12i, n_{Au} = 0.47 + 10.99i. The boundary condition is set as scattering boundary. α_{TBG} is related to the overlap integration of the in-plane electrical field of the hybrid mode and the TBG conductivity, which can be obtained by the following relationship [9]:

$$\alpha_{TBG} = 4.343 \times 10^{-6} \times \frac{1}{2} \times Real(\sigma_{TBG}) \times \left(\left|\vec{E_x}\right|^2 + \left|\vec{E_z}\right|^2\right) / \iint P(x,y)dxdy \quad (6)$$

where Real (σ_g) is the real part of the graphene conductivity, $\vec{E_x}$ and $\vec{E_z}$ is the x and z direction component of the electric fields along the TBG surface of the TE mode. $P(x,y)$ represents the average power at the coordinate (x,y) of the simulated waveguide.

We optimize the slab width and slot width of the TBG/silicon slot hybrid waveguide to reach the maximum absorption coefficient with different types of SOI wafers, as shown in Figure 3. We can find that the highest absorption coefficient α_{TBG} can be as high as 0.41 dB/μm when the slot width and slab width within the type-C SOI are chosen as 150 nm and 240 nm respectively. Moreover, for type-A and type-B SOI wafers, the highest α_{TBG} are both higher than 0.35 dB/μm.

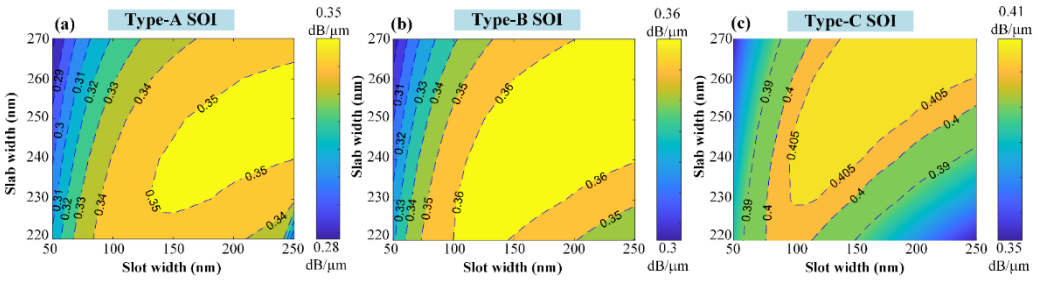

Figure 3. The absorption coefficients of TBG as a function of the slot width and slab width with different types of SOI wafers. (**a**) 260 nm silicon top layer with 1 μm BOX layer. (**b**) 250 nm silicon top layer with 3 μm BOX layer. (**c**) 220 nm silicon top layer with 2 μm BOX layer.

Several photodetection mechanism have been reported in monolayer graphene photodetectors including photovoltaic effect, photo-thermoelectric effect, and photo-bolometric effect [7]. For the photo-thermoelectric effect, the graphene layer requires to be doped differently. For the photo-bolometric effect, it strongly relies on the heat generation and accumulation process within the small volume. These conditions are not satisfied within the proposed photodetector. Therefore, the dominant photodetection mechanism of the TBG/silicon photodetector is the photovoltaic effect where TBG absorbs light and generates the electron-hole pairs. The electron-hole pairs are separated by the sum of built-in and external electric field and thus the photocurrent is generated. The responsivity (R) of the photodetector is defined as:

$$R = \frac{I_{ph}}{P_{in}} \tag{7}$$

where I_{ph} is the photocurrent while P_{in} is the power of the input light. The photocurrent I_{ph} can be expressed as [5]:

$$I_{ph} = qn^*\mu\xi L \tag{8}$$

where q is the elementary charge, n^* is the photo-induced carrier density, μ is the mobility of these carriers within graphene, ξ is the electric field and L is the length of the photodetector, which can be expressed as:

$$\xi = V_{ext}/d \tag{9}$$

where V_{ext} is the external bias voltage applied to the photodetector which is set as 1 V in the calculation. d is the distance of the electrode which is set as 2 μm in our design.

The formula for n^* can be written as:

$$n^* = M \times P_{ab} \times \tau_{rc}/(E_p \times L \times g) \tag{10}$$

where M is the carrier multiplication factor. Since there is no internal gain within the proposed photodetector, M is set as 1 in the calculation. τ_{rc} is the carrier recombination time, E_p is the energy of the incident photon, L is the length of the TBG/silicon slot waveguide and the g is the gap width. For simplicity, we assume that the photogenerated carriers are mainly concentrated within the gap region. The power of light P_{ab} which is absorbed by TBG, can be calculated by:

$$P_{ab} = P_{in} \times (1 - 10^{-(\alpha_{TBG} * L)/10}) \tag{11}$$

Based on the optimization process above, the α_{TBG} is set as 0.41 dB/μm and the dependence of the responsivity on the length of the photodetector and the wavelength of the incident light is also investigated as the blue curve shows in the Figure 4a. We can find that the responsivity increases with the length of the photodetector which is shorter than 30 μm. When the length continues to increase larger than 30 μm, the responsivity almost remains unchanged at its maximum value of 1.154 A/W. This phenomenon indicates that almost all the incident light is absorbed within the 30 μm. Moreover, this value suppresses all the graphene/silicon hybrid photodetector operating at the communication wavelength range, thanks to the enhancement of the TBG as well as the strong light-TBG interaction provided by the silicon slot waveguide. As a comparison, we replace the TBG with the monolayer graphene in the same waveguide structure in Figure 2 and calculate the corresponding responsivity. We can see that the highest responsivity remains lower than 0.3 A/W, which is close to the value reported in a similar structure [11]. This also demonstrates that TBG can significantly enhance the responsivity of the photodetector. Moreover, the I-V characteristic can be also calculated from the abovementioned model and the results are shown in Figure 4b. In the calculation, the length of the photodetector is set as 40 μm while the input light power is set as 1 mW. Meanwhile, we can find that the current increases when the light is injected into the photodetector, which verifies that the main photodetection mechanism is the photovoltaic effect.

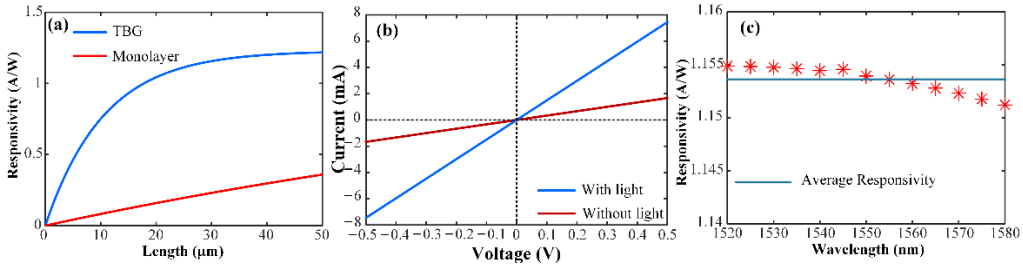

Figure 4. (**a**) The responsivity as a function of the length of the photodetector; (**b**) The I-V characteristic of the TBG photodetector (**c**) The responsivity as a function of the wavelength of the incident light.

Besides, the effect of the incident wavelength on the responsivity is also calculated as the Figure 4c displays. The mechanism of how the wavelength affects the responsivity can be divided into two parts. On one hand, the mode distribution within the TBG/silicon slot hybrid waveguide varies with different incident wavelengths, thus leading to the different absorption coefficient of TBG. On the other hand, since the enhancement of the optical conductivity of the TBG is dependent on the incident photon energy, which is shown in Figure 1, the wavelength can change the optical conductivity of the TBG thus affecting the responsivity of the photodetector. Here we consider both mechanisms above and find that the responsivity holds a high value and a good uniformity from 1520 nm to 1580 nm, indicating that the optical bandwidth of the proposed photodetector can cover the entire C-band of the optical communication systems. To expand the optical bandwidth of the photodetector to an even larger range such as the infrared wavelength (2 μm) or O-band wavelength (1.3 μm), one should not only tune the twisted angle of the TBG, but also optimize the structure parameters of the slot waveguide correspondingly to support the light with different wavelengths to propagate within the slot region waveguide.

2.4. The Electrical-Optical Response Calculation of the Silicon/TBG Photodetector

The electrical-optical bandwidth of the graphene photodetector is jointly determined by the photo-response time and the electric-circuit response time. Thanks to the ultra-short lifetime of the photogenerated carriers within twisted bilayer graphene [24], the photo-response limited bandwidth of the twisted bilayer graphene photodetector can be larger than 150 GHz. Therefore, the operation bandwidth is mainly limited by the electric-circuit response time. To analyze the 3-dB bandwidth of the silicon/TBG photodetector, we utilize the equivalent circuit model method as the Figure 5a displays.

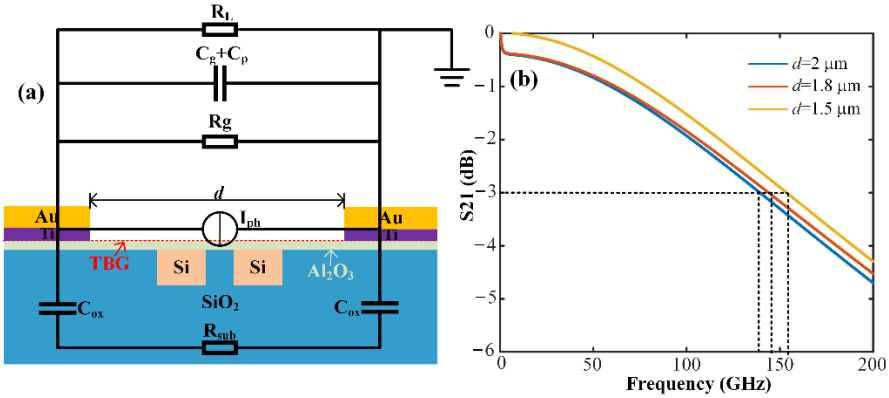

Figure 5. (**a**) The equivalent circuit model of the TBG/silicon photodetector. (**b**) The calculated electro-optical response S21 curve with different electrode distances.

In the calculation, R_L= 50 Ω represents the load resistance. C_g + C_p is the total capacitance of the circuit including the graphene capacitance and the metallic pad capacitance, respectively. C_{ox} is the capacitance of the buried oxide layer. R_{sub} is the resistance of the silicon substrate and R_g is the total resistance of the circuit, which can be calculated by:

$$R_g = R_c + \frac{d}{2L}\sigma_{TBG}^{-1} \tag{12}$$

where R_c is the contact resistance, d is the distance between the electrodes, L is the length of the photodetector and σ_{TBG} is the conductivity of TBG. The theoretical frequency response curve can be described by the relationships below [9]:

$$S_{21} = \left| \frac{Z_{in}}{Z_{in} + R_L} \right| \tag{13}$$

$$Z_{in}(f) = \frac{\frac{R_g}{j2\pi f R_g(C_g+C_p)+1}\left(R_{sub} + \frac{1}{j2\pi f 2C_{ox}}\right)}{\frac{R_g}{j2\pi f R_g(C_g+C_p)+1} + R_{sub} + \frac{1}{j2\pi f 2C_{ox}}} \tag{14}$$

The S21 curves of the TBG/silicon photodetector with different electrode distances d are shown in Figure 5b. The calculated 3-dB bandwidth of the photodetector with d of 2 μm is 139.2 GHz, which indicates that the TBG/silicon photodetector also holds the advantages of ultrahigh operation bandwidth, comparing to the silicon slot waveguide photodetector with monolayer graphene exhibiting 3-dB bandwidth lower than 100 GHz [11,25]. Moreover, we could see that the 3-dB bandwidth of the proposed silicon/TBG increases with narrower electrode distance, owing to the smaller channel resistance. It should be pointed out that highest experimentally verified responsivity and bandwidth of the monolayer graphene/silicon hybrid photodetector operating at 1550 nm are 0.6 A/W and 110 GHz respectively [25,26]. However, these values are lower than their theoretical calculated values. The main factors that lead to the discrepancy in simulations and the experiments includes the quality of the graphene sheet, the coupling and propagation loss of the waveguide, the contaminations induced during the fabrication process as well as the fabrication error. Same situations could be expected in the proposed TBG/silicon slot waveguide photodetector.

3. Discussion

The fabrication process of the TBG/silicon slot hybrid photodetector starts with the electron beam lithography (EBL) and ICP etch to fabricate the passive opponents of the photodetector including the grating coupler, the strip waveguide, the coupler between the strip waveguide and the slot waveguide as well as the slot waveguide. Afterwards, SiO_2 is deposited onto the chip using the plasma enhanced chemical vapor deposition (PECVD). Next the chemical mechanical polish (CMP) process is employed to planarize the chip before completing the transfer process of the TBG. Since the quality of the TBG is sensitive to the surface condition of the waveguide, unplanarized waveguide surface may lead to the crack of the TBG, thus causing the poor performance of the photodetector. Several methods have been proposed to transfer the TBG with the specific angle onto the substrate, including the stacking method, the selective pick-up and transfer method and the controlled folding method. After the TBG transfer, the UV lithography process is used to pattern the TBG exposure and O_2 plasma etch to remove the useless part of the TBG. The final step is to fabricate the metal contact as well as the electrodes through the photoresist deposition, UV exposure, electron beam evaporation and lift-off process subsequently. In the proposed device, the large-area growth of twisted bilayer graphene acts as a crucial step. Several methods have been reported to obtain high-quality A-B stacked bilayer graphene with accurate twist angle including the hetero-site nucleation [20], CVD growth on Cu/Ni(111) foil [27] and the angle replication method [28].

To investigate the fabrication tolerance of the TBG/silicon hybrid photodetector, we first calculate the TBG conductivity under different twisted angle is first calculated using Equations (3)–(5). Afterwards, the TBG absorption coefficient (α_{TBG}) as a function of the deviation angle is calculated through Equation (6) combining the mode distribution withing the absorption region. With the αTBG, one can obtain the responsivity as a function of the deviation angle based on the Equations (7)–(11). as Figure 6 shows. We could see that the responsivity remains higher than 1 A/W when the twisted angle deviation from

the designed twisted angle is 1°, which indicates that good fabrication tolerance of the proposed device. Moreover, we can also conclude that the accuracy control of the twisted angle significantly affects the responsivity of the graphene photodetector and one should ensure that the twisted angle is identical to the designed value in the fabrication process.

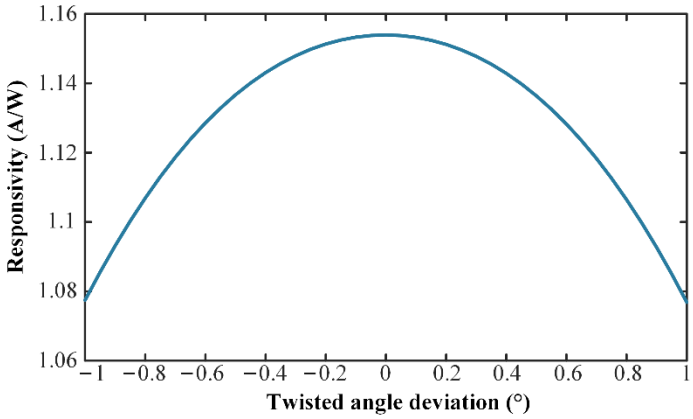

Figure 6. The responsivity as a function of the twisted angle deviation.

4. Conclusions

In this work, we theoretically demonstrated a high-performance silicon/TBG hybrid integrated photodetector operating at 1550 nm. Thanks to the significantly enhanced absorption of TBG as well as the comprehensive optimization of the TBG/silicon hybrid waveguide, the highest responsivity of the photodetector reaches 1.154 A/W, featuring the highest responsivity compared to the reported graphene photodetector operating at communication wavelength range. The silicon/TBG photodetector also holds an ultrahigh bandwidth of 139.2 GHz, ensuring its ability to be operated in the ultrafast optical communication systems. Besides, the fabrication process of the photodetector and its fabrication error tolerance are also discussed, indicating a good CMOS compatibility and fabrication error tolerance. This work paves the way for the practical applications of the TBG in the optical communication field and provides valuable theoretical basis for its future design and fabrication.

Author Contributions: Conceptualization, S.Y. and Y.D.; Data curation, W.W., Y.Y. and X.Z.; Funding acquisition, S.Y. and Y.D.; Supervision, S.Y., M.T. and Y.D.; Visualization, Y.Z., S.H., W.P. and X.P.; Writing—original draft, S.Y., Y.Y., X.Z. and Z.Z. (Ziwen Zhou); Writing—review & editing, Y.Y., S.H., X.P., Z.Z. (Ze Zhang), M.T., S.Y. and Y.D. All authors have read and agreed to the published version of the manuscript.

Funding: This research was funded by National Natural Science Foundation of China (No. 62205114), the Key Research and Development Program of Hubei Province (No. 2022BAA001), Starting Research Fund from the Huazhong University of Science and Technology (No. 3004182179); the National Undergraduate Training Projects for Innovation and Entrepreneurship (No. 5003182104); VILLUM FONDEN (No. 00025298).

Data Availability Statement: The data presented in this study are available on request from the corresponding author.

Conflicts of Interest: The authors declare no conflict of interest.

References

1. Agrawal, G.P. *Fiber-Optic Communication Systems*; John Wiley & Sons: New York, NY, USA, 2012; Volume 222.
2. Zhang, L.; Udalcovs, A.; Lin, R.; Ozolins, O.; Pang, X.; Gan, L.; Schatz, R.; Tang, M.; Fu, S.; Liu, D. Toward terabit digital radio over fiber systems: Architecture and key technologies. *IEEE Commun. Mag.* **2019**, *57*, 131–137. [CrossRef]
3. Xue, Y.; Han, Y.; Tong, Y.; Yan, Z.; Wang, Y.; Zhang, Z.; Tsang, H.K.; Lau, K.M. High-performance III-V photodetectors on a monolithic InP/SOI platform. *Optica* **2021**, *8*, 1204–1209. [CrossRef]

4. Lischke, S.; Peczek, A.; Morgan, J.; Sun, K.; Steckler, D.; Yamamoto, Y.; Korndörfer, F.; Mai, C.; Marschmeyer, S.; Fraschke, M. Ultra-fast germanium photodiode with 3-dB bandwidth of 265 GHz. *Nat. Photonics* **2021**, *15*, 925–931. [CrossRef]
5. Rouvalis, E.; Chtioui, M.; van Dijk, F.; Lelarge, F.; Fice, M.J.; Renaud, C.C.; Carpintero, G.; Seeds, A.J. 170 GHz uni-traveling carrier photodiodes for InP-based photonic integrated circuits. *Opt. Express* **2012**, *20*, 20090–20095. [CrossRef] [PubMed]
6. Freitag, M.; Low, T.; Xia, F.; Avouris, P. Photoconductivity of biased graphene. *Nat. Photonics* **2013**, *7*, 53–59. [CrossRef]
7. Koppens, F.; Mueller, T.; Avouris, P.; Ferrari, A.; Vitiello, M.; Polini, M. Photodetectors based on graphene, other two-dimensional materials and hybrid systems. *Nat. Nanotechnol.* **2014**, *9*, 780–793. [CrossRef]
8. Ding, Y.; Cheng, Z.; Zhu, X.; Yvind, K.; Dong, J.; Galili, M.; Hu, H.; Mortensen, N.A.; Xiao, S.; Oxenløwe, L.K. Ultra-compact integrated graphene plasmonic photodetector with bandwidth above 110 GHz. *Nanophotonics* **2020**, *9*, 317–325. [CrossRef]
9. Guo, J.; Li, J.; Liu, C.; Yin, Y.; Wang, W.; Ni, Z.; Fu, Z.; Yu, H.; Xu, Y.; Shi, Y. High-performance silicon–graphene hybrid plasmonic waveguide photodetectors beyond 1.55 μm. *Light Sci. Appl.* **2020**, *9*, 29. [CrossRef]
10. Ma, Z.; Kikunaga, K.; Wang, H.; Sun, S.; Amin, R.; Maiti, R.; Tahersima, M.H.; Dalir, H.; Miscuglio, M.; Sorger, V.J. Compact graphene plasmonic slot photodetector on silicon-on-insulator with high responsivity. *ACS Photonics* **2020**, *7*, 932–940. [CrossRef]
11. Wang, J.; Cheng, Z.; Chen, Z.; Wan, X.; Zhu, B.; Tsang, H.K.; Shu, C.; Xu, J. High-responsivity graphene-on-silicon slot waveguide photodetectors. *Nanoscale* **2016**, *8*, 13206–13211. [CrossRef]
12. Schuler, S.; Muench, J.E.; Ruocco, A.; Balci, O.; Thourhout, D.v.; Sorianello, V.; Romagnoli, M.; Watanabe, K.; Taniguchi, T.; Goykhman, I. High-responsivity graphene photodetectors integrated on silicon microring resonators. *Nat. Commun.* **2021**, *12*, 3733. [CrossRef] [PubMed]
13. Yan, S.; Zuo, Y.; Xiao, S.; Oxenløwe, L.K.; Ding, Y. Graphene photodetector employing double slot structure with enhanced responsivity and large bandwidth. *Opto-Electron. Adv.* **2022**, *5*, 210159. [CrossRef]
14. Sato, K.; Saito, R.; Cong, C.; Yu, T.; Dresselhaus, M.S. Zone folding effect in Raman *G*-band intensity of twisted bilayer graphene. *Phys. Rev. B* **2012**, *86*, 125414. [CrossRef]
15. Yankowitz, M.; Chen, S.; Polshyn, H.; Zhang, Y.; Watanabe, K.; Taniguchi, T.; Graf, D.; Young, A.F.; Dean, C.R. Tuning superconductivity in twisted bilayer graphene. *Science* **2019**, *363*, 1059–1064. [CrossRef] [PubMed]
16. Kerelsky, A.; McGilly, L.J.; Kennes, D.M.; Xian, L.; Yankowitz, M.; Chen, S.; Watanabe, K.; Taniguchi, T.; Hone, J.; Dean, C. Maximized electron interactions at the magic angle in twisted bilayer graphene. *Nature* **2019**, *572*, 95–100. [CrossRef] [PubMed]
17. Yu, K.; Van Luan, N.; Kim, T.; Jeon, J.; Kim, J.; Moon, P.; Lee, Y.H.; Choi, E. Gate tunable optical absorption and band structure of twisted bilayer graphene. *Phys. Rev. B* **2019**, *99*, 241405. [CrossRef]
18. Yin, J.; Wang, H.; Peng, H.; Tan, Z.; Liao, L.; Lin, L.; Sun, X.; Koh, A.L.; Chen, Y.; Peng, H. Selectively enhanced photocurrent generation in twisted bilayer graphene with van Hove singularity. *Nat. Commun.* **2016**, *7*, 10699. [CrossRef]
19. Deng, B.; Ma, C.; Wang, Q.; Yuan, S.; Watanabe, K.; Taniguchi, T.; Zhang, F.; Xia, F. Strong mid-infrared photoresponse in small-twist-angle bilayer graphene. *Nat. Photonics* **2020**, *14*, 549–553. [CrossRef]
20. Sun, L.; Wang, Z.; Wang, Y.; Zhao, L.; Li, Y.; Chen, B.; Huang, S.; Zhang, S.; Wang, W.; Pei, D. Hetero-site nucleation for growing twisted bilayer graphene with a wide range of twist angles. *Nat. Commun.* **2021**, *12*, 2391. [CrossRef]
21. Dos Santos, J.L.; Peres, N.; Neto, A.C. Graphene bilayer with a twist: Electronic structure. *Phys. Rev. Lett.* **2007**, *99*, 256802.
22. Ha, S.; Park, N.H.; Kim, H.; Shin, J.; Choi, J.; Park, S.; Moon, J.-Y.; Chae, K.; Jung, J.; Lee, J.-H.; et al. Enhanced third-harmonic generation by manipulating the twist angle of bilayer graphene. *Light Sci. Appl.* **2021**, *10*, 19. [CrossRef] [PubMed]
23. Ma, C.; Yuan, S.; Cheung, P.; Watanabe, K.; Taniguchi, T.; Zhang, F.; Xia, F. Intelligent infrared sensing enabled by tunable moiré quantum geometry. *Nature* **2022**, *604*, 266–272. [CrossRef] [PubMed]
24. Patel, H.; Huang, L.; Kim, C.-J.; Park, J.; Graham, M.W. Stacking angle-tunable photoluminescence from interlayer exciton states in twisted bilayer graphene. *Nat. Commun.* **2019**, *10*, 1445. [CrossRef] [PubMed]
25. Wen, P.; Tiwari, P.; Mauthe, S.; Schmid, H.; Sousa, M.; Scherrer, M.; Baumann, M.; Bitachon, B.I.; Leuthold, J.; Gotsmann, B.; et al. Waveguide coupled III-V photodiodes monolithically integrated on Si. *Nat. Commun.* **2022**, *13*, 909. [CrossRef]
26. Lee, S.; Cheng, C.W.; Sun, X.; Emic, C.D.; Miyazoe, H.; Frank, M.M.; Lofaro, M.; Bruley, J.; Hashemi, P.; Ott, J.A.; et al. High Performance InGaAs Gate-All-Around Nanosheet FET on Si Using Template Assisted Selective Epitaxy. In Proceedings of the 2018 IEEE International Electron Devices Meeting (IEDM), San Francisco, CA, USA, 1–5 December 2018; pp. 39.35.31–39.35.34.
27. Huang, M.; Bakharev, P.V.; Wang, Z.-J.; Biswal, M.; Yang, Z.; Jin, S.; Wang, B.; Park, H.J.; Li, Y.; Qu, D. Large-area single-crystal AB-bilayer and ABA-trilayer graphene grown on a Cu/Ni (111) foil. *Nat. Nanotechnol.* **2020**, *15*, 289–295. [CrossRef]
28. Liu, C.; Li, Z.; Qiao, R.; Wang, Q.; Zhang, Z.; Liu, F.; Zhou, Z.; Shang, N.; Fang, H.; Wang, M. Designed growth of large bilayer graphene with arbitrary twist angles. *Nat. Mater.* **2022**, *21*, 1263–1268. [CrossRef]